Lawrence Berkeley National Laboratory

Title

Accessing Lanthanide-to-Lanthanide Energy Transfer in a Family of Site-Resolved [LnIIILnIII′] Heterodimetallic Complexes

Authors

Galán, Laura Abad
Aguilà, David
Guyot, Yannick
et al.

Peer reviewed

Accessing Lanthanide-to-Lanthanide Energy Transfer in a Family of Site-Resolved [Ln(III)Ln(III)'] Heterodimetallic Complexes

Laura Abad Galán,#[a, b] David Aguilà,#[c, d] Yannick Guyot,[e] Verónica Velasco,[c, d] Olivier Roubeau,[f] Simon J. Teat,[g] Massimiliano Massi*[a] and Guillem Aromí*[c, d]

[a]   Dr. L. Abad Galán, Dr. M. Massi
        School of Molecular and Life Sciences and Curtin Institute for Functional Molecules and Interfaces
        Curtin University
        Kent Street, Bentley 6102 WA, Australia
        E-mail: m.massi@curtin.edu.au
[b]   Dr. L. Abad Galán
        Univ Lyon, ENS de Lyon, CNRS UMR 5182
        Université Claude Bernard Lyon 1,
        F-69342 Lyon, France
[c]   Dr. D. Aguilà, Dr. V. Velasco, Dr. G. Aromí
        Departament de Química Inorgànica i Orgànica
        Universitat de Barcelona
        Diagonal 645, 08028 Barcelona, Spain
        E-mail: guillem.aromi@qi.ub.edu
[d]   Dr. D. Aguilà, Dr. V. Velasco, Dr. G. Aromí
        Institute of Nanoscience and Nanotechnology
        University of Barcelona (IN2UB), 08007 Barcelona, Spain
[e]   Dr. Yannick Guyot
        Univ Lyon, Institut Lumière Matière, UMR 5306 CNRS
        Université Claude Bernard Lyon 1
        Rue Ada Byron, F-69622 Villeurbanne Cedex, France
[f]   Dr. O. Roubeau
        Instituto de Nanociencia y Materiales de Aragón (INMA)
        CSIC and Universidad de Zaragoza
        Plaza San Francisco s/n, 50009, Zaragoza, Spain
[g]   Dr. S. J. Teat
        Advanced Light Source, Berkeley Laboratory
        1Cyclotron Road, Berkeley,California, 94720, USA

Supporting information for this article is given via a link at the end of the document. # L.A.G and D.A contributed equally.

Abstract: The ligand H_3L (6-(3-oxo-3-(2-hydroxyphenyl)propionyl)-pyridine-2-carboxylic acid), which exhibits two different coordination pockets, has been exploited to engender and study energy transfer (ET) in two dinuclear [Ln(III)Ln(III)'] analogues of interest, [EuYb] and [NdYb]. Their structural and physical properties have been compared with the also newly synthesised analogues featuring no possible ET ([EuLu], [NdLu] and [GdYb], respectively) and with the corresponding homometallic [EuEu] and [NdNd] analogues, previously reported. Photophysical data suggest that ET between Eu(III) and Yb(III) does not occur to a significant extent, while emission from Yb(III) originates via sensitization from the ligand. In contrast, energy migration seems to be occurring between the two Nd(III) centers in [NdNd], as well as in [NdYb], where Yb(III) luminescence is thus in part sensitised by ET from Nd. This study shows the versatility of this molecular platform to further the investigation of lanthanide-to-lanthanide ET phenomena in defined molecular systems.

Introduction

Lanthanides have contributed enormously towards the development of advanced materials and technologies, including catalysts, magnetic and electronic devices, telecommunication systems, lasers, wind and solar energy conversion materials as well as medical applications.[1-25] The potential towards these technologies derives from their characteristic optical and magnetic properties.[26, 27] Among those, their unique photophysical features such as their line-like emission spectra and long-lived excited state decays have particular relevance. In addition, their emission wavelengths span the visible range, as red europium -Eu(III)- or green terbium -Tb(III)-, to the near infrared range (NIR) with examples such as neodymium -Nd(III)- or ytterbium -Yb(III)-.[27-29] NIR emission stands out notably due to its potential application for night vision devices, telecommunications and life sciences.[1, 3-5, 30, 31] Nevertheless, triggering direct intra-configurational *f-f* transitions is hindered by the very low molar absorptivity of lanthanide ions. The latter is the case because these transitions are parity forbidden when mediated by the electric dipole operator, while the magnetically induced ones are very weak (due to the low magnitude of the magnetic dipole operator in most lanthanides). In addition, the transitions are often also

1

spin forbidden. To alleviate this problem, π-conjugated organic ligands (and to a more limited extent metal-organic chromophores, *ie.* complexes of a different metal near the target Ln ion)[32, 33] have been routinely used as sensitisers of lanthanide emission.[15, 34-44] These chromophores act by efficiently harvesting photons, and then transferring the energy to the lanthanide ions, usually after intersystem crossing. This process is more generally known as the antenna effect. Alternatively, other mechanisms such as energy transfer (ET) between different lanthanide ions can also be considered, which often results in improved sensitisation efficiencies, also enhancing the range of absorption and emission wavelengths.[45-51] Such Ln-to-Ln sensitization is very useful for up-conversion phenomena, which allow the conversion of low energy photons into photons of higher energy[52, 53] or down-conversion, where the energy transfer transforms photons from higher to lower energy. However, this particular approach to sensitisation is by far less studied, mainly restricted to co-doped crystals, ceramics and glasses.[54-57] There are however some remarkable examples of homometallic or heterometallic Ln-to-Ln ET studies taking place within discrete molecules.[35, 48, 58-66] Most of them are conducted in solution, with polydentate ligands in the presence of two different lanthanide ions.[67-69] In many of these systems, there is little-to-no control on the location of each Ln(III) in the molecular scaffold, as is mainly dictated by statistical speciation.[35] However, very interesting studies relying on site-selectivity have been performed in heterometallic compounds obtained through consecutive synthetic steps,[61-63, 70-77] or in a rare molecular system featuring different metallic environments, but lacking selectivity.[48, 58] The scarce number of examples of selective systems obtained thermodynamically from one pot reactions reflect on the difficulties in developing molecular materials with more than one type of lanthanide ion, predictably distributed at selected positions within the molecular scaffold in one-step. These problems are the consequence of the very similar chemical behavior within this series of metals. In this context, in the last years we have developed a ligand-based strategy to promote dinuclear heterometallic [Ln(III)Ln(III)'] lanthanide compounds with a distribution of two 4f ions that can be highly selective in many cases.[78] Such control was achieved using the asymmetric H₃L ligand (H₃L = 6-(3-oxo-3-(2-hydroxyphenyl)propionyl)-pyridine-2-carboxylic acid), which exhibits two different coordination pockets (Scheme 1). One is a O,O-type β-diketonate chelate (when deprotonated) and the other a O,N,O dipicolinate one. The former exhibits two closely lying donor atoms and favors shorter Ln–O distances than the other pocket, with more separate O-donor atoms. The combination of this ligand with any lanthanide ion was found first to produce a comprehensive series of asymmetric dinuclear homometallic [Ln(III)Ln(III)] compounds for the entire 4f series: (Hpy)[Ln₂(HL)₃(NO₃)(py)(H₂O)].[79] This study allowed a detailed crystallographic investigation, revealing that the bond distances between the oxygen donor atoms and each Ln (Scheme 1, Ln1, and Ln2) are systematically larger for site 2 (Ln2) when compared to site 1 (Ln1). This suggested the possibility to produce

heterometallic [Ln(III)Ln(III)'] compounds with high purity in many cases by combining two Ln ions with different ionic radii, expecting the smaller one to selectively coordinate to the position suited for shorter Ln-O bonds (site 1) and the larger one in site 2 (where longer Ln-O bonds are preferred). This approach successfully led to several (Hpy)[LnLn'(HL)₃(NO₃)(py) (H₂O)] compounds with unprecedented purity and featuring various [Ln(III)Ln(III)'] combinations.[78, 80-82]

This molecular platform thus furnishes an ideal scenario to study and evaluate the nature of lanthanide-to-lanthanide ET phenomena, with the additional benefit that this family of complexes is characterised by a relatively short distance (around 3.8 Å) between both lanthanide ions. This distance is very favorable for efficient ET, since it allows the mechanisms that require orbital overlap (*ie.* Dexter energy transfer)[34] in addition to dipolar through-space pathways.[83, 84] Following this strategy, a series of five new heterometallic complexes [EuYb] (**1**), [NdYb] (**2**), [EuLu] (**3**), [NdLu] (**4**), [GdYb] (**5**) were synthesised and photophysically characterised. This family allowed investigation of visible-to-NIR ET in [EuYb], as well as NIR-to-NIR ET in [NdYb] to a great level of detail. Indeed, the photophysical properties of these systems could be directly compared with their homometallic ([EuEu] and [NdNd]) and heterometallic ([EuLu], [NdLu] and [GdYb]), analogues the latter including examples where no ET processes can occur.
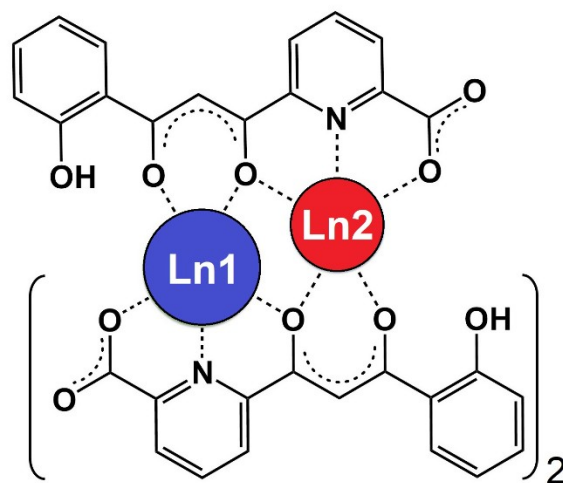
Scheme 1. Schematic representation of the complex anion in (Hpy) [Ln1Ln2(HL)₃(NO₃)(py)(H₂O)], emphasizing the coordination environment produced by the ligands and the two different cavities of the system (site 1 for Ln1 (red) and site 2 for Ln2 (blue)).

Results and Discussion

Synthesis. Considering the remarkable difference between the ionic radii of Nd(III) or Eu(III) with respect to Yb(III), both [EuYb] (**1**) and [NdYb] (**2**) compounds were expected to exhibit a selective metallic distribution. In order to complete the study and evaluate the properties that each individual metal would have in these two molecules, [EuLu] (**3**), [NdLu] (**4**) and [GdYb] (**5**) complexes were also synthesized. The five heterometallic compounds were obtained following the same procedure reported for the previous [Ln(III)Ln(III)']

systems.[78, 80, 81] Thus, three equivalents of H_3L were mixed in pyridine with one equivalent of the nitrate salt of each of the two required lanthanides under aerobic conditions. Slow diffusion of diethyl ether into the resulting solutions afforded yellow needle-like crystals of $(Hpy)[LnLn'(HL)_3(NO_3)(py)(H_2O)]$ in moderate yields (see Experimental Section), as expected from previous studies. Each compound was evaluated by elemental analysis, as well as by SCXRD and MS, supporting its essentially heterometallic nature (see below).

Structural characterization. The five new compounds are quasi-isostructural and crystallize in the monoclinic $P2_1/c$ space group (Table S1). The asymmetric unit exhibits one $[LnLn'(HL)_3(NO_3)(py)(H_2O)]^-$ anion, one pyridinium cation (Hpy^+) and four (or five for compound **4**) molecules of pyridine. The structure shows three twice-deprotonated HL^{2-} ligands wrapping the two lanthanide ions in a helicoidal manner with a head-to-head-to-tail conformation (Figure 1). This consequently produces two different coordination sites with distinct encapsulation features. Site 1 is formed by two β−diketonate (O,O) chelating pockets and one dipicolinate-like unit (O,N,O). Nonacoordination around the Ln^{3+} ion at this site is completed by one molecule of water and one of pyridine, respectively. On the other hand, site 2 is produced by one β−diketonate unit and two dipicolinate-like donors, together with a NO_3^- ligand. For compounds **1**, **3** and **5** ([EuYb], [EuLu] and [GdYb], respectively) the latter exhibits a monodentate coordination mode, providing a coordination number nine to the Ln^{3+} ion (Figures 1, top, S1 and S2). In contrast, for compounds **2** and **4** ([NdYb] and [NdLu]), the NO_3^- anion shows a bidentate mode due to the larger size of the Nd^{3+} ion, promoting ten-coordination at site 2 (Figures 1, bottom, and S3). The negative charge of these anionic complexes is compensated in all compounds by the pyridinium cation, which interacts with one of the carboxylate groups of the complex through a H-bond (Figure S4).
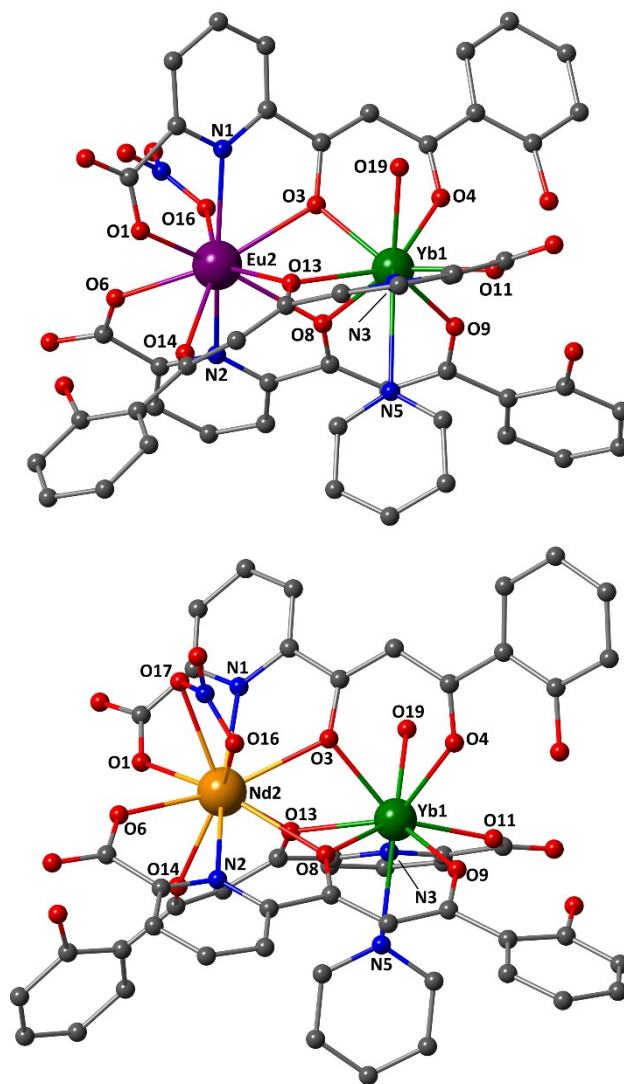

Figure 1. Representation of the anionic complex in compounds **1** ([EuYb], top) and **2** ([NdYb], bottom). Eu, Nd, Yb, C, N and O atoms are shown in purple, orange, green, grey, blue and red, respectively. H atoms are not shown for clarity.

In order to determine the nature of the Ln(III) ion at each site, the crystal structure of each compound was refined by considering the four possible metallic distributions: heterometallic with site 2 featuring the largest cation, heterometallic with site 1 encapsulating the largest cation, and both possible homometallic systems. The most representative agreement factors (R_1, wR_2 and S) as well as the displacement parameters were collected for each case. The data for compounds of the type [LnYb] (**1**, **2** and **5**) are shown in Table S2, while compounds **3** and **4** ([LnLu]) are evaluated in Table S3. As expected, based on the significant differences in ionic radii, all complexes show best refinement parameters for a heterometallic system where the largest Ln^{3+} is encapsulated in site 2. In contrast, the inversed distribution of the ions shows the worst agreement.

Considering these distributions, the average of the Ln–O bond distances involving the O donor atoms (Tables S4 and S5) from the HL^{2-} ligands, $avg.(Ln-O)$, were collected

and compared (Table 1). As expected, the *avg*.(Ln2-O) values in the [LnYb] compounds (2.44, 2.49 and 2.42 Å for [EuYb], [NdYb] and [GdYb], respectively) are considerably larger than the *avg*.(Yb1-O) ones (2.35, 2.36 and 2.35 Å, respectively). Similarly, [EuLu] and [NdLu] compounds exhibit larger *avg*.(Ln2-O) values (2.43 and 2.49 Å, respectively) than the ones observed for *avg*.(Lu1-O) (2.34 and 2.36 Å, respectively). It should be also noted that all the *avg*.(Ln-O) values found in compounds **1** - **5** are very similar to these observed in the corresponding sites for the respective homometallic dinuclear compounds,[79] and that they follow the expected trend derived from the lanthanide contraction (Table 1). However, the difference of average bond lengths between site 1 and site 2 (ΔO) in each heterometallic molecular system was found to be systematically larger than the one observed for their respective pair of homometallic compounds, evidencing the structural effect in this molecular scaffold when hosting two different Ln^{3+} ions with large and small ionic radii, respectively.

Once the nature of the lanthanide ion at each site determined, their corresponding coordination polyhedron was evaluated by means of Continuous Shape Measures (CShMs).[85, 86] Both lanthanide ions in compounds **1**, **3** and **5** ([EuYb], [EuLu] and [GdYb], respectively) are nine-coordinate, and were thus compared with ideal nine-vertex polyhedra (Table S6). The results show that site 1 can be described as a spherical capped square antiprism with C_{4v} symmetry or as a spherical tricapped trigonal prism (D_{3h}) symmetry. In contrast, no ideal polyhedron was found to accurately define with sufficient accuracy the low symmetry site 2, the closest one showing C_s symmetry described as "muffin". Similarly, the small lanthanide ions in site 1 for complexes [NdYb] (**2**) and [NdLu] (**4**) (Yb^{3+} and Lu^{3+}, respectively) show also coordination nine and are best defined as a spherical capped square antiprism or a spherical tricapped trigonal prism (Table S7). On the other hand, Nd^{3+}, encapsulated in site 2, is ten-coordinated, with very low symmetry as none of the ideal polyhedra can satisfactorily define the coordination environment. The closest ones are the sphenocorona (C_{2v}) and the staggered dodecahedron (D_2), respectively.

Mass spectrometry. Electrospray ionization mass spectrometry (ESI-MS) was used to explore the stability and selectivity of the compounds under discussion in solution. Experiments in a mixture of MeOH/DMSO indicate that the heterometallic nature for all **1** – **5** compounds is, in essence maintained, since the spectrograms show prominent peaks corresponding to the isotopic distribution of the heterometallic moiety observed in the solid state. Nevertheless, in some cases, additional peaks resulting from the corresponding homometallic analogues were also found in relatively small abundances. This feature results from a partial scrambling of the lanthanide ions in solution due to the dissociation of the H_2O, py and NO_3^- terminal ligands, which slightly relaxes the structure and therefore the selectivity, as previously observed and calculated by DFT for related analogues.[80, 81] For compounds **2** and **4**, where the difference between the ionic radii of the two Ln(III) ions is large, the signals for homometallic moieties are marginal (Figures 2 and S5). For compounds **1**, **3** and **5**, which feature a smaller size difference between the corresponding ions, the homometallic moieties are more visible, although still weaker than the heterometallic distribution (Figures S6 to S8). It must be considered that MS is not a quantitative analytical technique, since the relative intensity of the signals detected depends in part on how efficiently the particles associated to them reach the detector. Attempts to use of ^1H NMR to obtain information on the stability of the compounds in solution are hampered by the complexity of the spectra (Figs. S9 to S17). Illustrative examples are described in the following. The spectrum of [NdYb] (**2**) approximately incorporates the signals observed in that of [NdNd] plus additional resonances, with no systematic intensity variation. This can be explained by the fact that both possible immediate environments around Nd are present in both compounds (Figs. S10 and S11) and the results are thus consistent with the MS experiments. The same observation is made for the [EuYb] complex (as compared with [EuEu]) with additional weaker resonances (Figs. 12 and 13). This clearly suggests the presence of impurities, as was already inferred by MS. Interestingly, the same spectra collected in DMSO (Figs. 14 to 17) exhibit much higher complexity, revealing that the complexes are not stable in this solvent. The MS results indicate that 10% DMSO in methanol is not sufficient to cause this decomposition. A detailed analysis of the ^1H NMR spectra is beyond the scope of this paper, while the preliminary results do not contradict the conclusions reached here.

Table 1. Average Ln-O and Ln1···Ln2 values (Å) observed for compounds **1-5**. For comparison, the average Ln-O values of each Ln in the corresponding site for the respective homometallic dinuclear compounds have been included, as well as the Ln···Ln separations.[79]

	[EuYb] (1)	[NdYb] (2)	[EuLu] (3)	[NdLu] (4)	[GdYb] (5)	[EuEu](site 2)	[NdNd](site 2)	[GdGd](site 2)	[YbYb](site 1)
avg.(Ln2-O)	2.44	2.49	2.43	2.49	2.42	2.46	2.50	2.43	---
avg.(Ln1-O)	2.35	2.36	2.34	2.36	2.35	---	---	---	2.34
Ln1···Ln1	3.7656(9)	3.8229(6)	3.7556(8)	3.8196(7)	3.7530(9)	3.8173(8)	3.8814(5)	3.8038(11)	3.7245(7)

Table 2. Photophysical summary data for the europium containing complexes.

	Media	λ_{em}/nm	τ_{obs}(Eu^{3+})/μs	τ_R [a] (Eu^{3+})/μs	Φ_{ln}^{ln}(Eu^{3+})
	Solid	675[b] + 980[c]	-	-	-
[EuYb] (1)	MeOH	675[b] + 980[c]	-	-	-
	Glass	616[d] + 980[c]	597	1070	0.558
	Solid	675[b]	-	-	-
[EuEu]	MeOH	675[b]	-	-	-
	Glass	616[d]	578	930	0.622
[EuLu] (3)	Glass	616[d]	512	1070	0.479
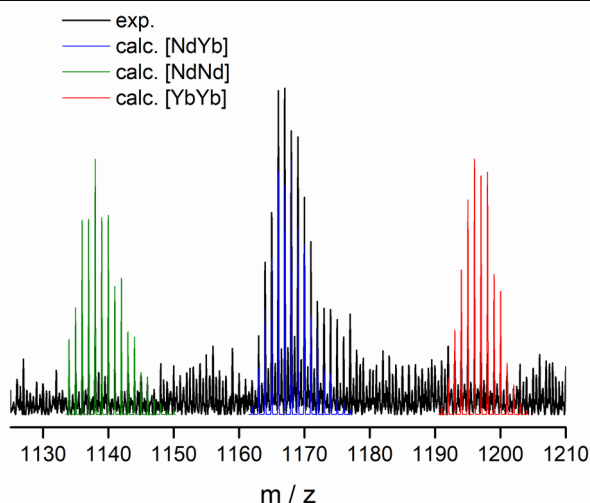
Figure 2. Selected region of the experimental (black line) ESI-MS spectra of compound **2** ([NdYb]), together with the calculated signals corresponding to [NdYb] (blue line), [NdNd] (green line) and [YbYb] (red line), which emphasizes the absence of homometallic fragments in the experimental plot.

Photophysical properties. Compounds **1** to **5** were prepared as an excellent platform to investigate ET between different Ln^{3+} centers within a molecular framework. Thus, an extensive investigation of the photophysical properties of these dinuclear lanthanide compounds has been carried out. Compounds [EuYb] (**1**) and [NdYb] (**2**) were thus selected as ideal to investigate visible-to-NIR and NIR-to-NIR ET phenomena, respectively. In the case of **1**, the expected energy transfer would potentially occur from the $^5D_0$ excited state of Eu(III) to the $^2F_{5/2}$ excited state of Yb(III). In order to determine the occurrence of ET, a comparison with the photophysical properties of the compound [EuEu] (the synthesis of which had been previously reported)[79] and of the new [EuLu] (**3**) analogue was performed. On the other hand, with compound **2** ET was anticipated to take place from the $^4F_{3/2}$ state of Nd(III) to the $^2F_{5/2}$ state of Yb(III). Similarly to **1**, a direct photophysical comparison was accomplished with the previously published compound [NdNd][79] and with the new complex [NdLu] (**4**). Finally, [GdYb] (**5**) was also investigated in order to have a reference compound presenting exclusive emission from Yb(III) via sensitisation from the organic chromophore (*i.e.* the ligand). The photophysical properties were investigated in the solid state and as diluted methanolic solution at room temperature, as well as at 77 K in some instances. These studies included the excitation and emission spectra as well as the lifetime decays for each compound at their maximum emission wavelength. A summary of the photophysical data is compiled in Tables 2 and 3.

Before any ET mechanism was studied, the triplet state of the HL^{2-} ligand was established. With this purpose, the emission of the previously synthesized [GdGd][79] analogue was measured at room temperature and at 77 K in methanolic solution. The phosphorescent emission band was enhanced in the frozen matrix and could thus be distinguished from the fluorescent emission, more predominant at room temperature (Figure 3). Deconvolution of the phosphorescent band (Figure S18) allowed evaluation of the energy of the triplet state of the ligand as the 0-phonon transition at ~19,050 cm^{-1}. This energy is sufficiently high to sensitise the emission from the $^4F_{3/2}$ state of Nd(III) (~11,260 cm^{-1}) and from the $^2F_{5/2}$ state of Yb(III) (~10,250 cm^{-1}). On the other hand, it is close to the energy of the $^5D_1$ and $^5D_0$ states of Eu(III) (~19,000 and ~17,200 cm^{-1}, respectively), hence some back energy transfer (BET) might be expected.

[a] Calculated from the emission spectrum following Eq. 1. [b] Ligand emission. [c] Yb^{3+} emission. [d] Eu^{3+} emission.

Visible-to-NIR Energy Transfer. To investigate ET between Eu(III) and Yb(III), the previously published [EuEu] complex was first analysed as a reference. The emission spectra in the solid state and in methanol at room temperature clearly show a broad band corresponding to the phosphorescent emission of the ligand, along with sharper peaks originating from the Eu(III) ion (Figures S19 and S20). This result indicates that thermally activated BET might be occurring at room temperature. Generally, a difference of at least 2,500 cm^{-1} is required to provide efficient energy transfer between the triplet state of a ligand and the excited state of a Ln(III) ion with no BET.[87] The close proximity between the ligand triplet state and the Eu(III) accepting states does therefore justify the presence of BET.
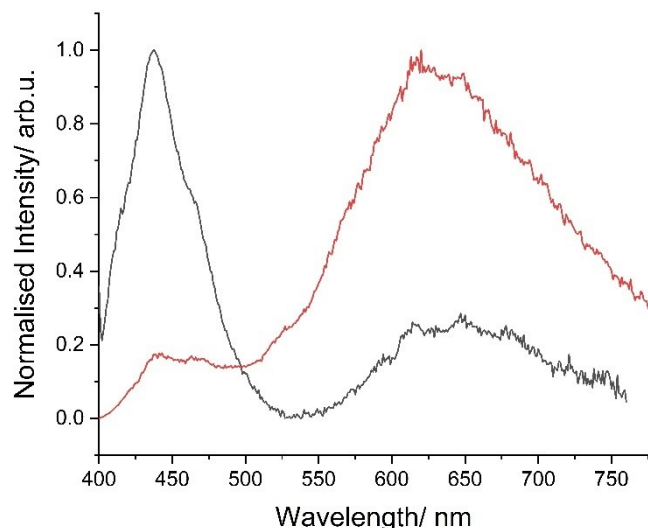
Figure 3. Emission spectra of [GdGd] (λ_{exc}= 375 nm) in methanol at room temperature (black trace) and 77K (red trace).

Figure 4. Normalised excitation (λ_{em}= 616 nm) (black trace) and emission (λ_{exc}= 375 nm) (red trace) spectra of [EuEu] in methanol at 77K. Insight: zoom of the $^5D_0$ to $^7F_0$ and $^7F_1$ transitions, respectively.

To verify this hypothesis, the emission spectrum was recorded in a frozen matrix at 77 K. In this case, the spectrum displays exclusively emission from the Eu(III) cation (Figure 4).

The broad excitation spectra recorded in all cases, spanning an analogous wavelength range as the absorption spectrum of the ligand, supports the conclusion that the Eu(III) emission is sensitised by the ligand. The emission spectrum presents the characteristic Eu(III) like line bands that can be attributed to the series of $^7F_J\leftarrow{}^5D_0$ (J = 0 - 4) transitions in the region of 550 - 725 nm (Figure 4).[88] The peak at 577 nm corresponds to the $^7F_0\leftarrow{}^5D_0$ transition, only observed when Eu(III) occupies a low symmetry site, as it is the case for both Eu(III) centres in this molecule. Since the crystal structure shows that the two Eu^{3+} ions occupy non-identical positions, two peaks are expected for this transition. In fact, the observed transition results into a relatively broad peak that can be fitted with two Gaussian functions centered at 17,275 and 17,262 cm^{-1} with full-width at half-maximum (FWHM) of 25 and 17 cm^{-1}, respectively (Figure S21). In this emission spectrum, the magnetic dipole allowed transition ($^7F_1\leftarrow{}^5D_0$) is observed between 585 and 600 nm. The splitting of this band was best fitted to four Gaussian functions (Figure S22), indicating the presence of more than one centre in this molecule, as the maximum splitting for one unique centre is three.[88] The observed excited state lifetime decay at 616 nm was fitted with a mono-exponential function with a value of 578 μs (Figure S23).
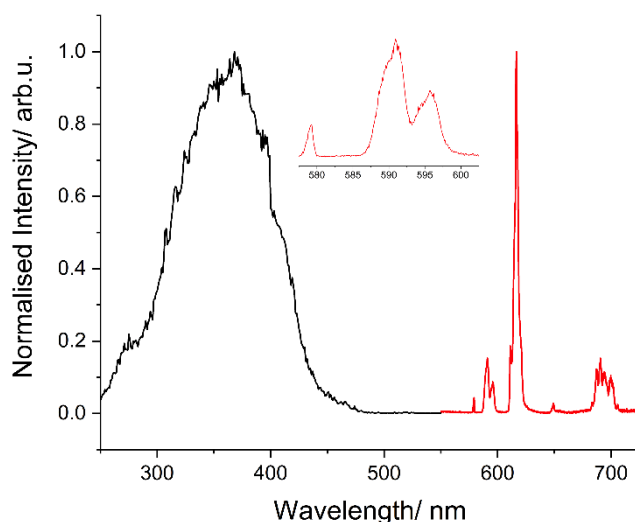
Similar results were obtained for the analogous photophysical study of the [EuLu] (**3**) complex (Figures S24 to S26). In this case, one unique $^7F_0\leftarrow{}^5D_0$ transition is observed at 17,272 cm^{-1} with a FWHM of 36 cm^{-1} (Figure S27). Meanwhile, the $^7F_1\leftarrow{}^5D_0$ band splits in three different peaks, which agrees with a unique Eu^{3+} ion with C_1 symmetry (Figure S28). These data further confirm the that the heterometallic nature of [EuLu] is retained solution, confirming that the presence of the homometallic moieties previously detected by mass spectrometry is only marginal (see above). The excited state lifetime decay at 616 nm was satisfactorily fitted with a mono-exponential function with a value of 512 μs (Figure S23), comparable to that observed for [EuEu]. The similarity between the lifetime values seems to suggest that intramolecular Eu-Eu energy migration is not a dominant process, in accordance with previous examples where the europium centres occupy non-identical positions.[83] However, in order to be able to gain further information of the energy migration within the molecule, the lifetime measurements should be performed at various characteristic emission wavelengths specific for site 1 or site 2 individually, as previously presented in the literature.[89] Unfortunately, in our system no significant difference was found between the emission spectrum of [EuEu] and [EuLu] (Figure S23) and therefore, the presence or absence of Eu-Eu energy migration cannot be proven conclusively.

The emission spectra of [EuYb] (**1**) present similar trends in the visible region, with a mixture of ligand phosphorescence and Eu-centred peaks in the solid state and methanolic solution at room temperature, and exclusive emission from Eu(III) at 77 K (Figures 5, S29 and S30). Consistently with the structure, one unique $^7F_0\leftarrow{}^5D_0$ transition is observed at 17,263 cm^{-1} with a peak FWHM of 27 cm^{-1}, while the splitting of the $^7F_1\leftarrow{}^5D_0$ band could be assigned to three different peaks in agreement with the C_1 symmetry of the coordination site (Figures S31 to S33). The characteristic Yb(III) NIR centred emission from the $^2F_{7/2}\leftarrow{}^2F_{5/2}$ transition was observed in

6

the 900 - 1100 nm region (Figures 5, S29 and S30). The excitation spectra recorded while monitoring emission at 980 nm reveal the typically broad bands associated to the ligand, suggesting that the Yb(III) emission is sensitised by the organic chromophore (Figures S29 and S30). The excited state lifetime decay of the Eu(III) emission at 616 nm in [EuYb] was monoexponential and determined to be 597 μs (Figure S23). The lack of decrease in the excited state lifetime decay between [EuLn] (Ln(III) = Eu(III), Lu(III)) and [EuYb] suggests that no ET is occurring from Eu(III) to Yb(III). To further support the hypothesis that the Yb(III) emission is originating through sensitisation from the ligand, the newly synthesised [GdYb] (**5**) analogue was investigated. The excitation and emission spectra in the solid state and in methanol at room temperature (Figures S34 to S36) are comparable to those of [EuYb]. The study of the lifetime decays at 980 nm (Yb(III) emission) of both complexes, [EuYb] (2.05 μs, 1.66 μs) and [GdYb] (2.02 μs, 1.62 μs) in solution and the solid state respectively, also corroborate the absence of Eu-Yb energy transfer (Figures S37 and S38). If present, the emission intensity of Yb(III) in [EuYb] should increase during a short period of time, depending on the rate of the energy transfer, which is not the case.[90] In this case, the lifetime found for [EuYb] upon excitation at 375 nm (ligand centered) or at direct excitation of europium shows the absence of time rise. The excited state decays associated with the Yb(III) in the latter complex have comparable shape to these of [GdYb], where only sensitisation from the ligand can occur (Figures S37 to S39). The intrinsic quantum yield for the Eu(III) emission was found to be similar in all cases, ranging between 0.479 and 0.622. These values were estimated by determining the radiative decay from the emission spectra (Table 2). This extensive study allows to confirm that no visible-to-NIR ET takes place within the [EuYb] complex.

NIR-to-NIR Energy Transfer. The photophysical properties of the [NdNd] species were first investigated. The emission spectra found in the solid state and in methanol at room temperature show the characteristic Nd(III) bands corresponding to the transitions $^4I_J \leftarrow {}^4F_{3/2}$ (J = 9/2, 11/2, 13/2), with maxima at 910 nm, 1060 nm and 1350 nm, respectively (Figure 6). The excited state decay for the 1060 nm maximum was determined to be 189 ns and 154 ns in the solid state and solution, respectively (Figure S40). The relative short values of the Nd(III) excited state lifetimes can be explained by the high susceptibility to quenching by O–H oscillators, as can be proven by the enhancement of this value when measured in deuterated methanol. The possible molecule of methanol directly coordinated to the Nd(1) centre could also have an effect. Unfortunately, the q value cannot be calculated do to the simultaneous high dependent on the number of close diffusing C–H.[91]
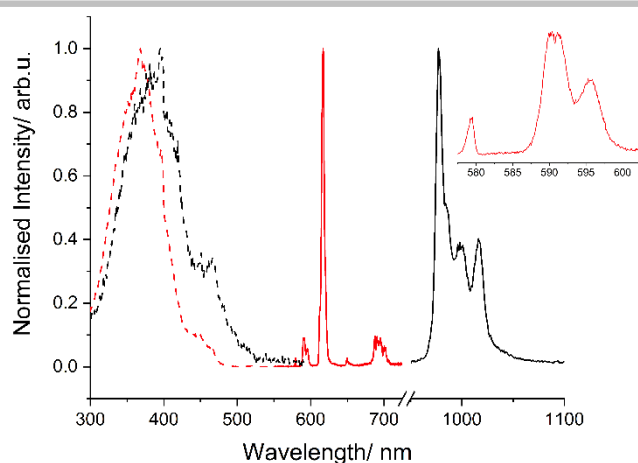

Figure 5. Normalised excitation at λ_{em} = 616 nm (dotted black trace) and λ_{em} = 980 nm (dashed red trace) and emission (λ_{exc}= 375 nm) (full red and black trace) spectra of [EuYb] (**2**) in methanol at 77 K.
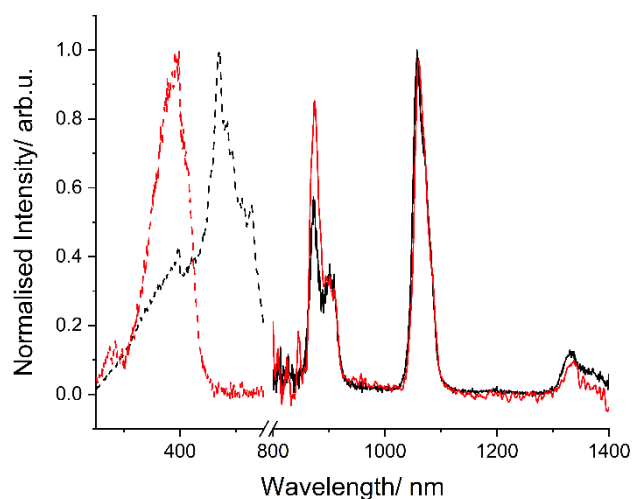

Figure 6. Normalised excitation (λ_{em}= 1060 nm) (dotted trace) and emission (λ_{exc}= 375 nm) (full trace) spectra of [NdNd] in the solid state (black trace) and in methanol (red trace) at room temperature.

Table 3. Photophysical summary data for the neodymium and ytterbium containing complexes.

[EuYb] (1)	Solid	675[b] + 980[c]	-	1.66	-	-
	Methanol	675[b] + 980[c]	-	2.05	492	0.004
[NdYb] (2)	Solid	980[c] + 1060[d]	183	1.58	-	-
	Methanol	980[c] + 1060[d]	143 (740)[e]	1.98 (32.52)[e]	615	0.003
[NdNd]	Solid	1060[d]	189	-	-	-
	Methanol	1060[d]	154 (961)[e]	-	-	-
[NdLu] (4)	Solid	1060[d]	331	-	-	-
	Methanol	1060[d]	178 (1097)[e]	-	-	-
[GdYb] (5)	Solid	980[c]	-	1.62	-	-
	Methanol	980[c]	-	2.02	454	0.004

[a] Calculated from the emission spectrum following Eq. 2. [b] Ligand emission. [c] Yb^{3+} emission. [d] Nd^{3+} emission. [e] lifetime measured in MeOD.

The analogue [NdLu] (**4**) was also synthesised to investigate energy migration between the two Nd(III) ions. The emission spectra (Figures S41 and S42) are comparable to those of [NdNd], with particularly longer lifetimes in the solid state (331 ns) and only modestly (178 ns) in solution, respectively (Figure S43). These differences suggest that the photophysical properties of [NdNd] could be influenced by cross relaxation mechanisms between the two lanthanide ions, which could be explained by a greater overlap between the absorption and emission spectra of both Nd(III) centres than seen for the Eu(III) ions in [EuEu].[89] The emission spectra for [NdYb] (**2**) in the solid state and in methanol at room temperature show emission from both Yb(III) and Nd(III) (Figure 7). While the emission of Yb(III) may have been sensitised by the excited state of Nd(III), the ligand can also directly sensitise the $^2F_{7/2} \leftarrow ^2F_{5/2}$ transition of this emissive center, as shown before. The lifetime decays of Nd(III) in [NdYb] (**2**) at 1060 nm were calculated at values of 183 ns and 143 ns for the solid state and in methanol solution, respectively (Figure S44). These values are also slightly shorter than the decays found for [NdLu] (**4**) where no energy transfer is possible, suggesting ET from Nd(III) to Yb(III). To corroborate this hypothesis, the Yb(III) lifetime decay was also measured in the solid state (1.58 μs) as well as in MeOH (1.98 μs) and MeOD (32.52 μs), giving a q value of 1 in correspondence to the crystal structure (Figure S44 and S45). The excited state lifetime enhancement seen in MeOD, was also observed for the Nd(III) emission line (961, 1097 and 740 ns for [NdNd], [NdLu] and [NdYb], respectively; Figures. S46, S47 and S48). After excitation of the ligand (375 nm) a subtle rise-time was observed in the solid state as well as solution at room temperature (Figure 8 and S44). This time rise was clearly more pronounced upon direct excitation of Nd(III) (584 nm) in the solid state (Figure 8). The presence of this time rise is suggestive of ET as it has been previously demonstrated in the literature[92-94] with other lanthanide pairs such as Tb-Eu.[90] The time rise was then fit to 80, 60 and 200 ns for the solid state, MeOH and MeOD solution, respectively, by use of Eq. 7 (Figures S49 to S51). Since these values are shorter than the corresponding lifetime decays of Nd(III), the Nd-to-Yb ET does not take place to completion, and other deactivating processes come simultaneously into play. Using Eq. 9, the ET efficiency is estimated to be 55%, 10% and 67% in the solid state, in MeOH and in MeOD solution, respectively. These differences underscore the effect of multiphonon deactivation also on ET rates.
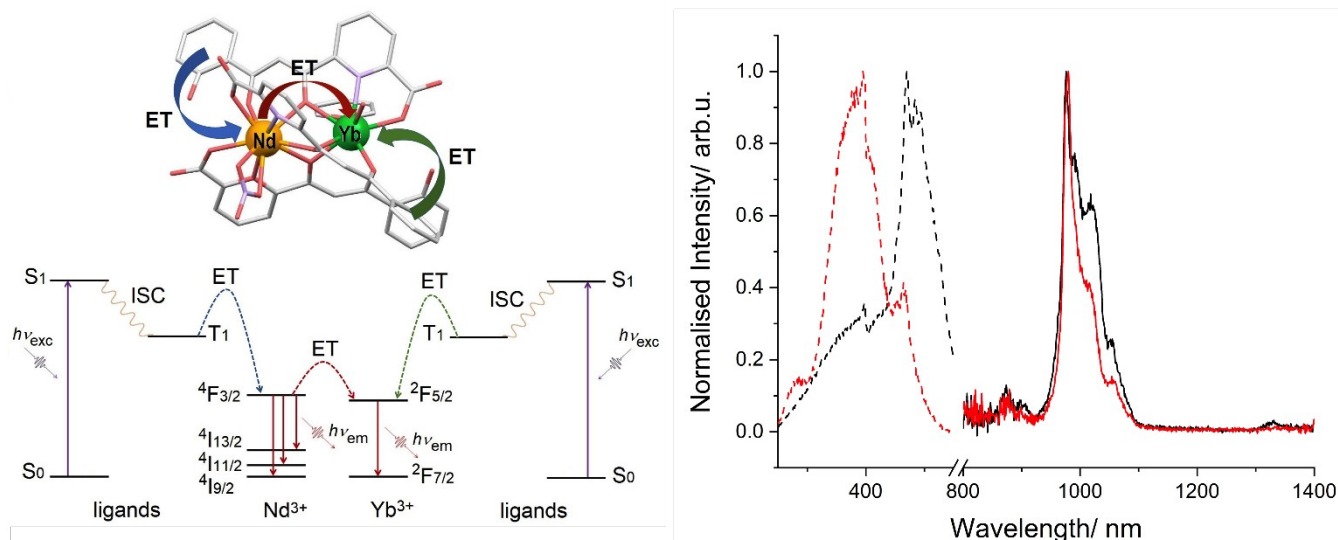
8

Figure 7. (Left) Schematic representation of the energy transfer phenomena in the [NdYb] (**2**) compound (top) and the corresponding terms and levels (bottom). (Right) Normalised excitation (λ_{em} = 980 nm) (dotted trace) and emission (λ_{exc}= 375 nm) (full trace) spectra of **2** in the solid state (black trace) and in methanol (red) at room temperature.
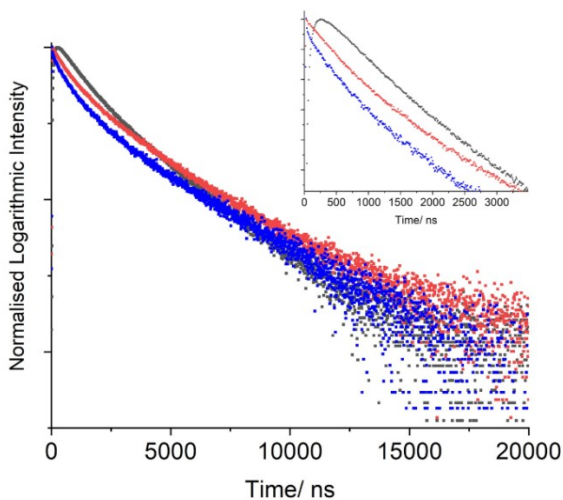

Figure 8. Decay of [NdYb] with λ_{exc}= 584 nm (black trace), [NdYb] with λ_{exc}= 375 nm (red trace) and [GdYb] (λ_{exc}= 375 nm) (blue trace) at 980 nm in the solid state. Inset: zoom on time to highlight the rise time.
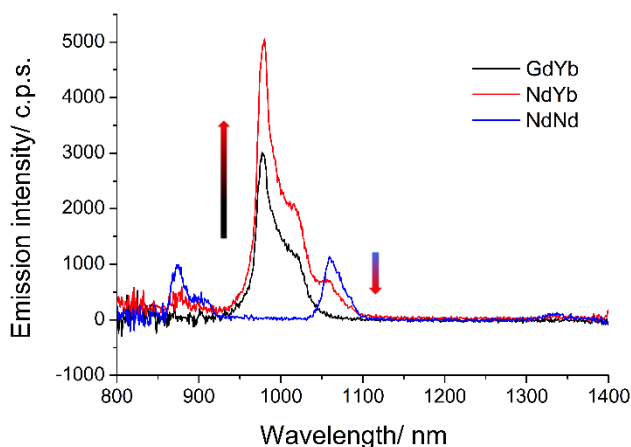

Figure 9. Emission spectra (λ_{exc}= 375 nm) of is absorbance solutions of **5** ([GdYb], black trace), **2** ([NdYb], red trace) and [NdNd] (blue trace) in methanol at room temperature.

Further corroboration of the analogous coordination geometry is the measured total splitting of the ground state $^2F_{7/2}$ of Yb(III) at low temperature, with very similar values of 390 cm^{-1}, 386 cm^{-1} and 371 cm^{-1} found respectively for the three complexes ([EuYb], [GdYb], and [NdYb], Figure S52). Moreover, the observable lifetime decays of these emissions were also found to be comparable, being 1.66 μs, 1.62 μs and 1.98 μs in the solid state or 2.05 μs , 2.02 μs and 2.26 μs in methanol at room temperature for [EuYb], [GdYb], and [NdYb], respectively. Through their radiative decays (Table 3), the sensitization efficiency for Yb(III) emission is estimated at similar values around 0.4%. The fact that the values of lifetime for the [NdYb] at 980 nm (Yb(III) emission) are comparable to those for the other Yb(III) containing species seems to suggest the absence of BET in [NdYb], which has previously been presented as a possible mechanism at room temperature for the quenching of this Yb(III) excited state.[55]

Conclusion

The ability of the versatile family of complexes with formulae (Hpy)[LnLn'(HL)$_3$(NO$_3$)(py)(H$_2$O)] to allocate with high selectivity two unequal lanthanide ions at two different positions of the molecule has been exploited to control and promote the Ln-to-Ln energy transfer phenomenon in a delivered manner. Five new [Ln(III)Ln(III)'] analogues have been synthesized and structurally characterized both in the solid state and in solution. These studies have corroborated the essentially heterometallic nature of each system. A comprehensive photophysical study has been performed to explore both visible-to-NIR and NIR-to-NIR energy transfer phenomena on the [EuYb] and [NdYb] analogues, respectively. The emission of both lanthanide ions in [EuYb] has been found to be sensitised only by the ligand, since no differences were observed when compared to [EuLu] (or [EuEu]) and [GdYb], respectively. In contrast, energy transfer from the $^4F_{3/2}$ state of Nd^{3+} to

the $^2F_{5/2}$ of Yb(III) has been observed for the [NdYb] compound, confirmed by the presence of a rise-time in the excited state decay of Yb(III) in [NdYb]. This work has demonstrated the versatile use of a versatile molecular platform that allows in-depth study of the lanthanide-to-lanthanide energy transfer.

Experimental Section

Synthesis

All reactions were performed in air, using the reagents as received. The ligand 6-(3-oxo-3-(2-hydroxyphenyl)propionyl)pyridine-2-carboxylic acid (H_3L) was synthesized according to the approach described previously by us.[95] Each [Ln(III)Ln(III)'] compound was synthesized following the same procedure reported for the previous [Ln(III)Ln(III)'] systems.[78, 80, 81]

(Hpy)[EuYb(HL)$_3$(NO$_3$)(py)(H$_2$O)] (1). A yellow solution of H_3L (30.0 mg, 0.105 mmol) in pyridine (10 mL) was added dropwise with stirring to a colorless solution of Eu(NO$_3$)$_3$·5H$_2$O (15.0 mg, 0.035 mmol) and Yb(NO$_3$)$_3$·5H$_2$O (15.7 mg, 0.035 mmol) in pyridine (10 mL). The resulting yellow solution was stirred for 2 h and layered with diethyl ether. After 1 week, yellow crystals of **1** were obtained (30 % yield). IR (KBr pellet): ṽ 3417 (mb), 1619 (s), 1585 (s), 1560 (m), 1527 (s), 1464 (m), 1400 (s), 1385 (s), 1326 (w), 1298 (m), 1239 (w), 1207 (w), 1147 (m), 1121 (w), 1059 (m), 950 (m), 756 (w), 707 (m), 665 (w), 635 (w). MS: m/z 1175.00 [EuYb(HL)$_2$(H$_2$L)]$^+$. Anal. Calcd for **1**·(-py)·4.7H$_2$O: C, 42.31; H, 3.15; N, 4.93. Found: C, 41.86; H, 2.67; N, 5.43.

(Hpy)[NdYb(HL)$_3$(NO$_3$)(py)(H$_2$O)] (2). A yellow solution of H_3L (30.0 mg, 0.105 mmol) in pyridine (10 mL) was added dropwise with stirring to a colorless solution of Nd(NO$_3$)$_3$·6H$_2$O (15.3 mg, 0.035 mmol) and Yb(NO$_3$)$_3$·5H$_2$O (15.7 mg, 0.035 mmol) in pyridine (10 mL). The resulting yellow solution was stirred for 2 h and layered with diethyl ether. After 1 week, yellow crystals of **2** were obtained (75 % yield). IR (KBr pellet): ṽ 3422 (mb), 1619 (s), 1584 (s), 1560 (m), 1528 (s), 1464 (m), 1401 (s), 1385 (s), 1326 (w), 1299 (m), 1239 (w), 1205 (w), 1148 (w), 1121 (w), 1058 (m), 951 (m), 892 (w), 762 (w), 707 (m), 664 (w), 636 (w), 569 (w). MS: m/z 1167.99 [NdYb(HL)$_2$(H$_2$L)]$^+$. Anal. Calcd for **2**·(-py)·2.5H$_2$O: C, 43.77; H, 2.94; N, 5.10. Found: C, 43.37; H, 2.65; N, 5.53.

(Hpy)[EuLu(HL)$_3$(NO$_3$)(py)(H$_2$O)] (3). A yellow solution of H_3L (30.0 mg, 0.105 mmol) in pyridine (10 mL) was added dropwise with stirring to a colorless solution of Eu(NO$_3$)$_3$·5H$_2$O (15.0 mg, 0.035 mmol) and Lu(NO$_3$)$_3$·5H$_2$O (15.8 mg, 0.035 mmol) in pyridine (10 mL). The resulting yellow solution was stirred for 2 h and layered with diethyl ether. After 1 week, yellow crystals of **3** were obtained (20 % yield). IR (KBr pellet): ṽ 3420 (mb), 1619 (s), 1586 (s), 1561 (m), 1529 (s), 1465 (m), 1400 (s), 1384 (s), 1300 (m), 1239 (w), 1209 (w), 1121 (w), 1061 (m), 947 (m), 893 (w), 756 (w), 708 (m), 669 (w), 637 (w), 569 (w). MS: m/z 1177.86 [EuLu(HL)$_2$(H$_2$L)]$^+$. Anal. Calcd for **3**(-py)·1.5H$_2$O: C, 44.03; H, 2.81; N, 5.14. Found: C, 43.54; H, 2.66; N, 5.63.

(Hpy)[NdLu(HL)$_3$(NO$_3$)(py)(H$_2$O)] (4). A yellow solution of H_3L (30.0 mg, 0.105 mmol) in pyridine (10 mL) was added dropwise with stirring to a colorless solution of Nd(NO$_3$)$_3$·6H$_2$O (15.3 mg, 0.035 mmol) and Lu(NO$_3$)$_3$·5H$_2$O (15.8 mg, 0.035 mmol) in pyridine (10 mL). The resulting yellow solution was stirred for 2 h and layered with diethyl ether. After 1 week, yellow crystals of **4** were obtained (20 % yield). IR: ṽ 3418 (mb), 1619 (s), 1584 (s), 1559 (m), 1530 (s), 1464 (m), 1402 (s), 1384 (s), 1300 (m), 1239 (w), 1201 (w), 1147 (m), 1120 (w), 1059 (m), 952 (m), 891 (w), 755 (w), 707 (m), 663 (w), 635 (w), 569 (w). MS: m/z 1169.00 [NdLu(HL)$_2$(H$_2$L)]$^+$. Anal. Calcd for **4**·(-py)·5H$_2$O: C, 42.32; H, 3.20; N, 4.94. Found: C, 41.60; H, 2.75; N, 5.76.

(Hpy)[GdYb(HL)$_3$(NO$_3$)(py)(H$_2$O)] (5). A yellow solution of H_3L (30.0 mg, 0.105 mmol) in pyridine (10 mL) was added dropwise with stirring to a colorless solution of Gd(NO$_3$)$_3$·6H$_2$O (15.8 mg, 0.035 mmol) and Yb(NO$_3$)$_3$·5H$_2$O (15.7 mg, 0.035 mmol) in pyridine (10 mL). The resulting yellow solution was stirred for 2 h and layered with diethyl ether. After 1 week, yellow crystals of 5 were obtained (45 % yield). IR: ṽ 3417 (mb), 1619 (s), 1585 (s), 1560 (m), 1529 (s), 1465 (m), 1401 (s), 1384 (s), 1325 (w), 1298 (m), 1239 (w), 1208 (w), 1121 (w), 1059 (m), 950 (m), 892 (m), 758 (w), 708 (m), 666 (w), 636 (w), 570 (w). MS: m/z 1181.02 [GdYb(HL)$_2$(H$_2$L)]$^+$. Anal. Calcd for **5**·(-py)·5.4H$_2$O: C, 41.78; H, 3.21; N, 4.87. Found: C, 41.23; H, 2.69; N, 5.44.

Single Crystal X-ray Diffraction

Data for compounds **2** and **4** were collected using a Bruker APEX II CCD diffractometer on the Advanced Light Source beamline 11.3.1 at Lawrence Berkeley National Laboratory, from a silicon 111 monochromator (λ = 0.7749 Å). Data reduction and absorption corrections were performed by using SAINT and SADABS, respectively.[96] Data for compounds **1**, **3** and **5** were collected on a single-axis HUBER diffractometer on station BM16 of the European Synchrotron Radiation Facility, Grenoble, France (λ = 0.738 Å). Cell refinement, data reduction and absorption corrections were done with HKL-2000 suite.[97] The structures were solved using SHELXT[98] and refined with full-matrix least squares on F^2 by using SHELXL-2014.[99] The heterometallic nature of the compounds was confirmed by evaluating the most representative agreement factors (R_1, wR_2 and S) as well as the displacement parameters of the corresponding lanthanides, considering the four possible combinations (LnLn', Ln'Ln, LnLn, and Ln'Ln') as summarized in **Tables S1** and **S2**. All details can be found in the supplementary crystallographic data for this paper in CIF format with CCDC numbers 2009856 (**1**), 2009857 (**2**), 2009858 (**3**), 2009859 (**4**) and 2009860 (**5**). These data can be obtained free of charge from The Cambridge Crystallographic Data Centre via www.ccdc.cam.ac.uk/data_request/cif.

Experimental details

Infrared spectroscopy. IR spectra were recorded in the range of 4000−400 cm^{-1} by using a Nicolet 5700 FT-IR spectrometer.

Mass spectrometry. Positive-ion ESI mass spectrometry experiments were performed by using a LC/MSD-TOF instrument (Agilent Technologies) with a dual source equipped with a lock spray for internal reference introduction, at the Unitat d'Espectrometria de Masses (SSR) from the Universitat de Barcelona. Experimental parameters: capillary voltage 4 kV, gas temperature 325 °C, nebulizing gas pressure 103.42 kPa, drying gas flow 7.0 L min^{-1}, and fragmentor voltage 175−250 V. Internal reference masses were m/z 121.05087 (purine) and 922.00979 (HP-0921). Samples were dissolved in a MeOH/DMSO mixture (μL) and introduced into the source by using a HPLC system (Agilent 110) with an H$_2$O/CH$_3$CN mixture (1/1) as the eluent (200 μL min^{-1}).

Elemental Analysis. C, H, and N analyses were performed by using a Thermo EA Flash 2000 (Thermo Scientific) analyzer at the Centres Cientiífcs i Tecnológics from the Universitat de Barcelona (CCiT-UB).

FULL PAPER

Photophysical Measurements. Absorption spectra were recorded at room temperature using a Perkin Elmer Lambda 35 UV/Vis spectrometer. Uncorrected steady state emission and excitation spectra were recorded using an Edinburgh FLSP980-stm spectrometer equipped with a 450 W xenon arc lamp, double excitation and emission monochromators, a Peltier cooled Hamamatsu R928P photomultiplier (185–850 nm) and a Hamamatsu R5509-42 photomultiplier for detection of NIR radiation (800-1400 nm). Emission and excitation spectra were corrected for source intensity (lamp and grating) and emission spectral response (detector and grating) by a calibration curve supplied with the instrument. Quantum yields were measured with the use of an integrating sphere coated with BenFlect.[100] Excited-state decays (τ) were recorded on the same Edinburgh FLSP980-stm spectrometer using a microsecond flashlamp, set at excitation wavelength of 350 nm, and monitored at the maximum emission wavelength being 980 nm, 1060 nm and 616 nm Yb^{3+}, Nd^{3+}, Eu^{3+} complexes, respectively. In the case of the Nd^{3+} derivatives excitation wavelength of 584 nm was also used to promote absorption to the $^4G_{5/2}$ and $^2G_{7/2}$ excited states of Nd^{3+}. The goodness of fit was assessed by minimizing the reduced χ^2 function and by visual inspection of the weighted residuals always from 40 ns onwards to remove the diffusion contribution of the 350 nm excitation beam. To record the luminescence spectra at 77 K, the samples were placed in quartz tubes (2 mm diameter) and inserted in a quartz Dewar filled with liquid nitrogen. All the solvents used in the preparation of the solutions for the photophysical investigations were of spectrometric grade.

Selected Equations

The values of the radiative lifetime (τ_R), and intrinsic quantum yield (Φ_{Ln}^{Ln}) can be calculated with the following equations.

$$\frac{1}{\tau} = 14.65 \, s^{-1} \times n^3 \times \frac{I_{Tot}}{I} \tag{1}$$

In equation 1, the refractive index (n) of the solvent is used (assumed value of 1.5 in the solid state). The value 14.65 s^{-1} is the spontaneous emission probability of the $^7F_1 \leftarrow {}^5D_0$ transition reported previously.[88] I_{Tot} is the total integrated intensity of the Eu^{3+} emission spectrum, and I_{MD} is the integrated intensity of the $^7F_1 \leftarrow {}^5D_0$ band.

$$\frac{1}{\tau} = 2303 \, x \, \frac{8 \pi c \, n^2 \, \check{v}^2 \, (2J+1)}{N_A (2J'+1)} \int \varepsilon(\check{v}) \, d\check{v} \tag{2}$$

In equation 2, N_A is Avogadro's number ($6.023 \square 10^{23}$ mol^{-1}), whereas J and J' are the quantum numbers for the ground and excited state of Yb^{3+}, respectively.[101]

$$\Phi_{Ln}^{Ln} = \frac{\tau_{obs}}{\tau} \tag{3}$$

In equation 3, τ_{obs} is the observed lifetime. Radiative and non-radiative constants can also be calculated from the radiative and observed lifetime decays, following equations 4 and 5.

$$\tau_{obs} = \frac{1}{k_r + k_{nr}} \tag{4}$$

$$\tau_r = \frac{1}{k_r} \tag{5}$$

The sensitization efficiency (η_{sens}) can be determined using equation 6, where Φ_{Ln}^L is the overall quantum yield obtained experimentally with an integrating sphere.

$$\eta_{sens} = \frac{\Phi_{Ln}^L}{\Phi_{Ln}^{Ln}} \tag{6}$$

The time-rise in the decay of Yb(III) at 1060 nm was fit using Equation 7.

$$I(t) = I_0 |\exp(-t/\tau) - \exp(-t/\tau_R)| \tag{7}$$

The rate of energy transfer (k_{ET}) and quantum efficiency of energy transfer (Φ_{ET}) can be calculated according to the following equations:

$$k_{ET} = \frac{1}{\tau} - \frac{1}{\tau} \tag{8}$$

$$\Phi_{ET} = 1 - \frac{\tau_q}{\tau} \tag{9}$$

where τ_q and τ_u are the $^4F_{3/2}$ decay lifetime of Nd^{3+} in the presence or absence of the quencher (Yb^{3+}), respectively.

[1]   S. V. Eliseeva, J.-C. G. Bünzli, *New J. Chem.* **2011**, *35*, 1165-1176.
[2]   J. Kido, Y. Okamoto, *Chem. Rev.* **2002**, *102*, 2357-2368.
[3]   S. V. Eliseeva, J.-C. G. Bünzli, *Chem. Soc. Rev.* **2010**, *39*, 189-227.
[4]   J. C. G. Bünzli, S. V. Eliseeva, in *Comprehensive Inorganic Chemistry II (Second Edition)* (Eds.: J. Reedijk, K. Poeppelmeier), Elsevier, Amsterdam, **2013**, pp. 339-398.
[5]   J.-C. G. Bünzli, in *Luminescence of Lanthanide Ions in Coordination Compounds and Nanomaterials* (Ed.: A. d. Bettencourt-Dias), John Wiley and Sons, Ltd, **2014**.
[6]   J.-C. G. Bünzli, *Eur. J. Inorg. Chem.* **2017**, *2017*, 5058-5063.
[7]   S. Shuvaev, M. Starck, D. Parker, *Chem., Eur. J.* **2017**, *23*, 9974-9989.
[8]   J.-C. G. Bünzli, K.-L. Wong, *J. Rare Earths* **2018**, *36*, 1-41.
[9]   J.-L. Liu, Y.-C. Chen, M.-L. Tong, *Chem. Soc. Rev.* **2018**, *47*, 2431-2453.
[10]   O. Cador, B. Le Guennic, F. Pointillart, *Inorg. Chem. Front.* **2019**, *6*, 3398-3417.
[11]   P. Martín-Ramos, M. R. Silva, *Lanthanide-based multifunctional materials : from OLEDs to SIMs*, Cambridge Elsevier, **2018**.
[12]   A. d. Bettencourt-Dias, *Luminescence of lanthanide ions in coordination compounds and nanomaterials*, Wiley, Chichester, U.K., **2014**.

[13] C.-H. Huang, *Rare Earth Coordination Chemistry: Fundamentals and Applications*, John Wiley & Sons (Asia) Pte Ltd, Singapore, **2010**.

[14] K. Binnemans, *Chem. Rev.* **2009**, *109*, 4283-4374.

[15] J.-C. G. Bünzli, *Chem. Rev.* **2010**, *110*, 2729-2755.

[16] C. P. Montgomery, B. S. Murray, E. J. New, R. Pal, D. Parker, *Acc. Chem. Res.* **2009**, *42*, 925-937.

[17] J.-C. G. Bünzli, *Interface focus* **2013**, *3*, 20130032.

[18] X. Chen, D. F. Peng, Q. Ju, F. Wang, *Chem. Soc. Rev.* **2015**, *44*, 1318-1330.

[19] H. Dong, L. D. Sun, C. H. Yan, *Chem. Soc. Rev.* **2015**, *44*, 1608-1634.

[20] X. H. Wang, H. J. Chang, J. Xie, B. Z. Zhao, B. T. Liu, S. L. Xu, W. B. Pei, N. Ren, L. Huang, W. Huang, *Coord. Chem. Rev.* **2014**, *273*, 201-212.

[21] H. C. Guo, S. Q. Sun, *Nanoscale* **2012**, *4*, 6692-6706.

[22] X. Chen, T. Y. Sun, F. Wang, *Chem., Asian J.* **2020**, *15*, 21-33.

[23] J. A. Briggs, A. C. Atre, J. A. Dionne, *J. Appl. Phys.* **2013**, *113*, 124509.

[24] P. Kumar, Kanika, S. Singh, R. Lahon, A. Gundimeda, G. Gupta, B. K. Gupta, *J. Lumin.* **2018**, *196*, 207-213.

[25] X. Y. Huang, S. Y. Han, W. Huang, X. G. Liu, *Chem. Soc. Rev.* **2013**, *42*, 173-201.

[26] A. Betencourt-Dias, in *Luminescence of Lanthanide Ions in Coordination Compounds and Nanomaterials*, Wiley, Singapore, **2014**, pp. 1-48.

[27] L. Ungur, in *Lanthanide-Based Multifunctional Materials* (Eds.: P. Martín-Ramos, M. Ramos Silva), Elsevier, **2018**, pp. 1-58.

[28] G. H. Dieke, H. M. Crosswhite, H. Crosswhite, *Spectra and Energy Levels of Rare Earth Ions in Crystals*, Interscience Publishers, **1968**.

[29] R. Hull, J. Parisi, R. Osgood, H. Warlimont, G. Liu, B. Jacquier, *Spectroscopic Properties of Rare Earth in Optical Materials, Vol. 83*, **2005**.

[30] J.-C. G. Bünzli, S. V. Eliseeva, *J. Rare Earths* **2010**, *28*, 824-842.

[31] V. V. Utochnikova, A. Grishko, A. Vashchenko, A. Goloveshkin, A. Averin, N. Kuzmina, *Eur. J. Inorg. Chem.* **2017**, *2017*, 5635-5639.

[32] L.-J. Xu, G.-T. Xu, Z.-N. Chen, *Coord. Chem. Rev.* **2014**, *273-274*, 47-62.

[33] F.-F. Chen, Z.-Q. Chen, Z.-Q. Bian, C.-H. Huang, *Coord. Chem. Rev.* **2010**, *254*, 991-1010.

[34] M. D. Ward, *Coord. Chem. Rev.* **2010**, *254*, 2634-2642.

[35] S. Lis, M. Elbanowski, B. Mąkowska, Z. Hnatejko, *J. Photochem. Photobiol. A* **2002**, *150*, 233-247.

[36] A. D'Aléo, C. Andraud, O. Maury, in *Luminescence of Lanthanide Ions in Coordination Compounds and Nanomaterials* (Ed.: A. Betencourt-Dias), Wiley, Singapore, **2014**, pp. 197-230.

[37] S. Faulkner, L. S. Natrajan, W. S. Perry, D. Sykes, *Dalton Trans.* **2009**, 3890-3899.

[38] W.-K. Wong, X. Zhu, W.-Y. Wong, *Coord. Chem. Rev.* **2007**, *251*, 2386-2399.

[39] A. D'Aléo, F. Pointillart, L. Ouahab, C. Andraud, O. Maury, *Coord. Chem. Rev.* **2012**, *256*, 1604-1620.

[40] J. Feng, H. Zhang, *Chem. Soc. Rev.* **2013**, *42*, 387-410.

[41] Y. Cui, Y. Yue, G. Qian, B. Chen, *Chem. Rev.* **2012**, *112*, 1126-1162.

[42] L. Armelao, S. Quici, F. Barigelletti, G. Accorsi, G. Bottaro, M. Cavazzini, E. Tondello, *Coord. Chem. Rev.* **2010**, *254*, 487-505.

[43] Y. Ma, Y. Wang, *Coord. Chem. Rev.* **2010**, *254*, 972-990.

[44] X.-S. Ke, B.-Y. Yang, X. Cheng, S. L.-F. Chan, J.-L. Zhang, *Chem., Eur. J.* **2014**, *20*, 4324-4333.

[45] D. T. de Lill, A. de Bettencourt-Dias, C. L. Cahill, *Inorg. Chem.* **2007**, *46*, 3960-3965.

[46] X. Rao, T. Song, J. Gao, Y. Cui, Y. Yang, C. Wu, B. Chen, G. Qian, *J. Am. Chem. Soc.* **2013**, *135*, 15559-15564.

[47] S. Freslon, Y. Luo, G. Calvez, C. Daiguebonne, O. Guillou, K. Bernot, V. Michel, X. Fan, *Inorg. Chem.* **2014**, *53*, 1217-1228.

[48] F. Artizzu, A. Serpe, L. Marchiò, M. Saba, A. Mura, M. L. Mercuri, G. Bongiovanni, P. Deplano, F. Quochi, *J. Mater. Chem., C* **2015**, *3*, 11524-11530.

[49] P. A. Tanner, L. Zhou, C. Duan, K.-L. Wong, *Chem. Soc. Rev.* **2018**, *47*, 5234-5265.

[50] S. Omagari, T. Nakanishi, Y. Kitagawa, T. Seki, K. Fushimi, H. Ito, A. Meijerink, Y. Hasegawa, *Sci. Rep.* **2016**, *6*, 37008.

[51] L. Song, Q. Wang, D. Tang, X. Liu, Z. Zhen, *New J. Chem.* **2007**, *31*, 506-511.

[52] F. Auzel, *Chem. Rev.* **2004**, *104*, 139-174.

[53] D. R. Gamelin, H. U. Güdel, *Acc. Chem. Res.* **2000**, *33*, 235-242.

[54] X. Wei, J. Zhao, W. Zhang, Y. Li, M. Yin, *J. Rare Earths* **2010**, *28*, 166-170.

[55] A. Lupei, V. Lupei, A. Ikesue, C. Gheorghe, S. Hau, *Optical Materials* **2010**, *32*, 1333-1336.

[56] B. Klimesz, R. Lisiecki, W. Ryba-Romanowski, *J. Lumin.* **2018**, *199*, 310-318.

[57] S. Stojadinović, R. Vasilić, *Mater. Lett.* **2019**, *234*, 9-12.

[58] F. Artizzu, F. Quochi, L. Marchiò, E. Sessini, M. Saba, A. Serpe, A. Mura, M. L. Mercuri, G. Bongiovanni, P. Deplano, *J. Phys. Chem. Lett.* **2013**, *4*, 3062-3066.

[59] L. Abad Galán, A. N. Sobolev, B. W. Skelton, E. Zysman-Colman, M. I. Ogden, M. Massi, *Dalton Trans.* **2018**, *47*, 12345-12352.

[60] L. Zhou, P. A. Tanner, W. Zhou, Y. Ai, L. Ning, M. M. Wu, H. Liang, *Angew. Chem., Int. Ed.* **2017**, *56*, 10357-10361.

[61] S. Faulkner, S. J. A. Pope, *J. Am. Chem. Soc.* **2003**, *125*, 10526-10527.

[62] N. Souri, P. Tian, C. Platas-Iglesias, K.-L. Wong, A. Nonat, L. J. Charbonnière, *J. Am. Chem. Soc.* **2017**, *139*, 1456-1459.

[63] A. Nonat, S. Bahamyirou, A. Lecointre, F. Przybilla, Y. Mély, C. Platas-Iglesias, F. Camerel, O. Jeannin, L. J. Charbonnière, *J. Am. Chem. Soc.* **2019**, *141*, 1568-1576.

[64] H. Yao, G. Calvez, C. Daiguebonne, K. Bernot, Y. Suffren, O. Guillou, *Inorg. Chem.* **2019**, *58*, 16180-16193.

[65] A. M. Nonat, L. J. Charbonnière, *Coord. Chem. Rev.* **2020**, *409*, 213192.

[66] S. N. Louise, *Curr. Inorg. Chem.* **2011**, *1*, 61-75.

[67] N. Andre, R. Scopelliti, G. Hopfgartner, C. Piguet, J. C. G. Bunzli, *Chem. Commun.* **2002**, 214-215.

[68] S. Floquet, M. Borkovec, G. Bernardinelli, A. Pinto, L.-A. Leuthold, G. Hopfgartner, D. Imbert, J.-C. G. Bünzli, C. Piguet, *Chem., Eur. J.* **2004**, *10*, 1091-1105.

[69] T. Riis-Johannessen, N. Dalla Favera, T. K. Todorova, S. M. Huber, L. Gagliardi, C. Piguet, *Chem., Eur. J.* **2009**, *15*, 12702-12718.

[70] M. S. Tremblay, D. Sames, *Chem. Commun.* **2006**, 4116-4118.

[71] I. Mamedov, T. N. Parac-Vogt, N. K. Logothetis, G. Angelovski, *Dalton Trans.* **2010**, *39*, 5721-5727.

[72] L. S. Natrajan, A. J. L. Villaraza, A. M. Kenwright, S. Faulkner, *Chem. Commun.* **2009**, 6020-6022.

[73] M. Suchý, A. X. Li, R. Bartha, R. H. E. Hudson, *Tetrahedron Lett.* **2010**, *51*, 1087-1090.

[74] M. P. Placidi, A. J. L. Villaraza, L. S. Natrajan, D. Sykes, A. M. Kenwright, S. Faulkner, *J. Am. Chem. Soc.* **2009**, *131*, 9916-9917.

[75] T. J. Sørensen, M. Tropiano, A. M. Kenwright, S. Faulkner, *Eur. J. Inorg. Chem.* **2017**, *2017*, 2165-2172.

[76] T. J. Sørensen, M. Tropiano, O. A. Blackburn, J. A. Tilney, A. M. Kenwright, S. Faulkner, *Chem. Commun.* **2013**, *49*, 783-785.

[77] T. J. Sørensen, S. Faulkner, *Acc. Chem. Res.* **2018**, *51*, 2493-2501.

[78] D. Aguilà, L. A. Barrios, V. Velasco, O. Roubeau, A. Repollés, P. J. Alonso, J. Sesé, S. J. Teat, F. Luis, G. Aromí, *J. Am. Chem. Soc.* **2014**, *136*, 14215-14222.

[79] D. Aguilà, L. A. Barrios, V. Velasco, L. Arnedo, N. Aliaga-Alcalde, M. Menelaou, S. J. Teat, O. Roubeau, F. Luis, G. Aromí, *Chem., Eur. J.* **2013**, *19*, 5881-5891.

[80] J. Gónzalez-Fabra, N. A. G. Bandeira, V. Velasco, L. A. Barrios, D. Aguilà, S. J. Teat, O. Roubeau, C. Bo, G. Aromí, *Chem., Eur. J.* **2017**, *23*, 5117-5125.

[81] D. Aguilà, V. Velasco, L. A. Barrios, J. González-Fabra, C. Bo, S. J. Teat, O. Roubeau, G. Aromí, *Inorg. Chem.* **2018**, *57*, 8429-8439.

[82] F. Luis, P. J. Alonso, O. Roubeau, V. Velasco, D. Zueco, D. Aguilà, J. I. Martínez, L. A. Barrios, G. Aromí, *Commun. Chem.* **2020**, *3*, 176.

[83] A. Zaïm, S. V. Eliseeva, L. Guénée, H. Nozary, S. Petoud, C. Piguet, *Chem., Eur. J.* **2014**, *20*, 12172-12182.

[84] F. Artizzu, F. Quochi, A. Serpe, E. Sessini, P. Deplano, *Inorg. Chem. Front.* **2015**, *2*, 213-222.

[85] A. Ruiz-Martínez, D. Casanova, S. Alvarez, *Chem., Eur. J.* **2008**, *14*, 1291-1303.

[86] A. Ruiz-Martínez, S. Alvarez, *Chem., Eur. J.* **2009**, *15*, 7470-7480.

[87] F. J. Steemers, W. Verboom, D. N. Reinhoudt, E. B. van der Tol, J. W. Verhoeven, *J. Am. Chem. Soc.* **1995**, *117*, 9408-9414.

[88] K. Binnemans, *Coord. Chem. Rev.* **2015**, *295*, 1-45.

[89] A. Nonat, M. Regueiro-Figueroa, D. Esteban-Gómez, A. de Blas, T. Rodríguez-Blas, C. Platas-Iglesias, L. J. Charbonnière, *Chem., Eur. J.* **2012**, *18*, 8163-8173.

[90] F. Baur, F. Glocker, T. Jüstel, *J. Mater. Chem., C* **2015**, *3*, 2054-2064.

[91] S. Faulkner, S. J. A. Pope, B. P. Burton-Pye, *Appl. Spectrosc. Rev.* **2005**, *40*, 1-31.

[92] S. P. Laptenok, J. W. Borst, K. M. Mullen, I. H. M. van Stokkum, A. J. W. G. Visser, H. van Amerongen, *Phys. Chem. Chem. Phys.* **2010**, *12*, 7593-7602.

[93] A. L. Feng, M. L. You, L. Tian, S. Singamaneni, M. Liu, Z. Duan, T. J. Lu, F. Xu, M. Lin, *Sci. Rep.* **2015**, *5*, 7779.

[94] N. M. Tart, D. Sykes, I. Sazanovich, I. S. Tidmarsh, M. D. Ward, *Photochem. Photobiol. Sci.* **2010**, *9*, 886-889.

[95] D. Aguilà, L. A. Barrios, F. Luis, A. Repollés, O. Roubeau, S. J. Teat, G. Aromí, *Inorg. Chem.* **2010**, *49*, 6784-6786.

[96] Bruker AXS Inc., Madison, WI, **2007**.

[97] Z. Otwinowski, W. Minor, in *Methods Enzymol., Vol. 276*, Academic Press, **1997**, pp. 307-326.

[98] G. Sheldrick, *Acta Cryst. A* **2015**, *71*, 3-8.

[99] G. Sheldrick, *Acta Cryst. C* **2015**, *71*, 3-8.

[100] J. C. de Mello, H. F. Wittmann, R. H. Friend, *Adv. Mater.* **1997**, *9*, 230-232.

[101] N. M. Shavaleev, R. Scopelliti, F. Gumy, J.-C. G. Bünzli, *Inorg. Chem.* **2009**, *48*, 7937-7946.

FULL PAPER

Entry for the Table of Contents
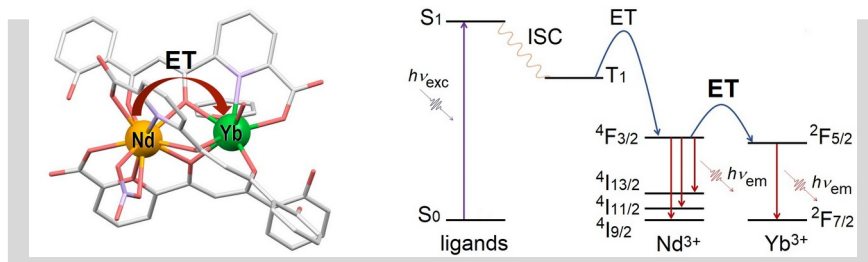
A new method to prepare a large number of different heterometallic [LnLn'] dinuclear complexes is exploited for a unique visible-to-NIR and NIR-to-NIR energy transfer within molecules, using the [EuYb] and the [NdYb] analogues, respectively. This has allowed to demonstrate intramolecular sensitization of Yb^{3+} by Nd^{3+}, acting as ET donor.

Institute and/or researcher Twitter usernames: @GMMF_UB